A Sigmoid Least Mean Fourth based Control Scheme for a Single-Stage Grid-Tied PV System

Abhisek Parida
Institute of Technology
Nirma University
Ahmedabad, India-382481
Email: abhisek.parida@nirmauni.ac.in

Bidyadhar Subudhi
School of Electrical Sciences
Indian Institute of Technology
Goa, Ponda, India-403401
Email: bidyadhar@iitgoa.ac.in

Pravat Kumar Ray
Department of Electrical Engineering
National Institute of Technology
Rourkela, India-769008
Email: rayp@nitrkl.ac.in

***Abstract*—In a single-stage grid-tied PV system, the Voltage Source Inverter (VSI) performs the task of MPPT along with delivery of high quality power to the grid. However, the presence of non-linear loads gives rise to Power Quality (PQ) issues in the distribution network. Therefore, it is necessary to develop a suitable control scheme for efficient functioning of the VSI. In this work, a Sigmoid Least Mean Fourth (SLMF) based control technique is discussed for a single-stage grid-tied PV system. The sigmoidal based adaptive algorithms embeds the conventional cost function into the sigmoidal framework to obtain improved performance by exploiting the saturation characteristics of the non-linear sigmoid function. The performance of the proposed SLMF based control scheme is simulated in MATLAB/Simulink under dynamic changes in load and environmental conditions and is compared with its conventional counterpart in terms of oscillation in weights and Total Harmonic Distortion (THD) of grid current.**

I. Introduction

Large powered photovoltaic (PV) installations are usualy grid-tied [1] thereby making effective utilization of solar power as compared to off-grid systems which need storage elements thus increasing the cost of the overall system. In a grid-tied PV system, the load demand is first fulfilled by the PV source and any additional load demand is met by the grid. When the load power demand is less than the the available PV power, the extra available power is injected to the grid. In a single-stage grid-tied PV system, there is a single power conversion stage (dc-ac) therby reducing the power loss as compared to a double-stage system which has two-power conversion stage and thus more number of components (diodes and capacitors) [2].

The connected loads at the Point of Common Coupling (PCC) of a grid-tied PV system may be linear requiring reactive compensation or non-linear which requires harmonic compensation in order to keep the THD of the grid currents within specified limits. Additionally, loads are continuously added and removed at the PCC which cause unbalancing of grid currents. All these factors lead to Power Quality (PQ) issues in the whole distribution system [3]. This has necessitated the development of efficient control techniques for switching of the Voltage Source Inverter (VSI) in order to mitigate the harmonics of the connected loads at the PCC along with delivery of high quality power to the grid.

A number of conventional control strategies for grid-tied systems make use of Phase Locked Loop (PLL) techniques to obtain the frequency and phase information of grid voltage in order to inject the grid current at same frequency and phase. Some of the PLL based techniques such as synchronous reference frame-PLL (SRF-PLL) [4], double SRF-PLL (DSRF-PLL), decoupled DSRF-PLL [5]. However, unbalance in grid voltage gives rise to erroneous phase information. Some advanced control techniques such as improved linear sinusoidal tracer (ILST), self-tuning filter (STF) etc., are presented in literature for PQ improvement in grid-tied PV system. The ILST and STF control schemes makes use of zero crossing detectors and sample and hold techniques to obtain the fundamental active components of the load current which increases the cost and complexity of the system. Apart from the prevalent techniques, adaptive filtering techniques such as Least Mean Fourth (LMF) [6], variable leaky least mean square (VLLMS) [7], combined infinite impulse response (IIR) and finite impulse response (FIR) filter [8] etc., are some of the adaptive control based schemes used for grid-tied PV systems because of its superior tracking capability during dynamic conditions. The conventional LMS and LMF algorithms suffer from convergence issue as it generates unbounded parameter estimates for bounded input. The combined IIR and FIR filter has delicate polynomials that leads to stability issues since small perturbations in co-efficients can make big changes in the roots. In this paper, a Sigmoid Least Mean Fourth (SLMF) based adaptive control strategy has been propsed which is an improved variant of the conventional LMF algorithm. By embedding the conventional cost function of the LMF algorithm into the sigmoidal framework thereby exploiting the saturation characteristics of non-linear sigmoid function, the drifting problem of LMF algorithm is solved which leads to improved performance. The cost function of the SLMF algorithm is given by Huang *et al.* [9]. The contributions of this work are summarized as follows:

- Proposed a new SLMF based control scheme for accu-

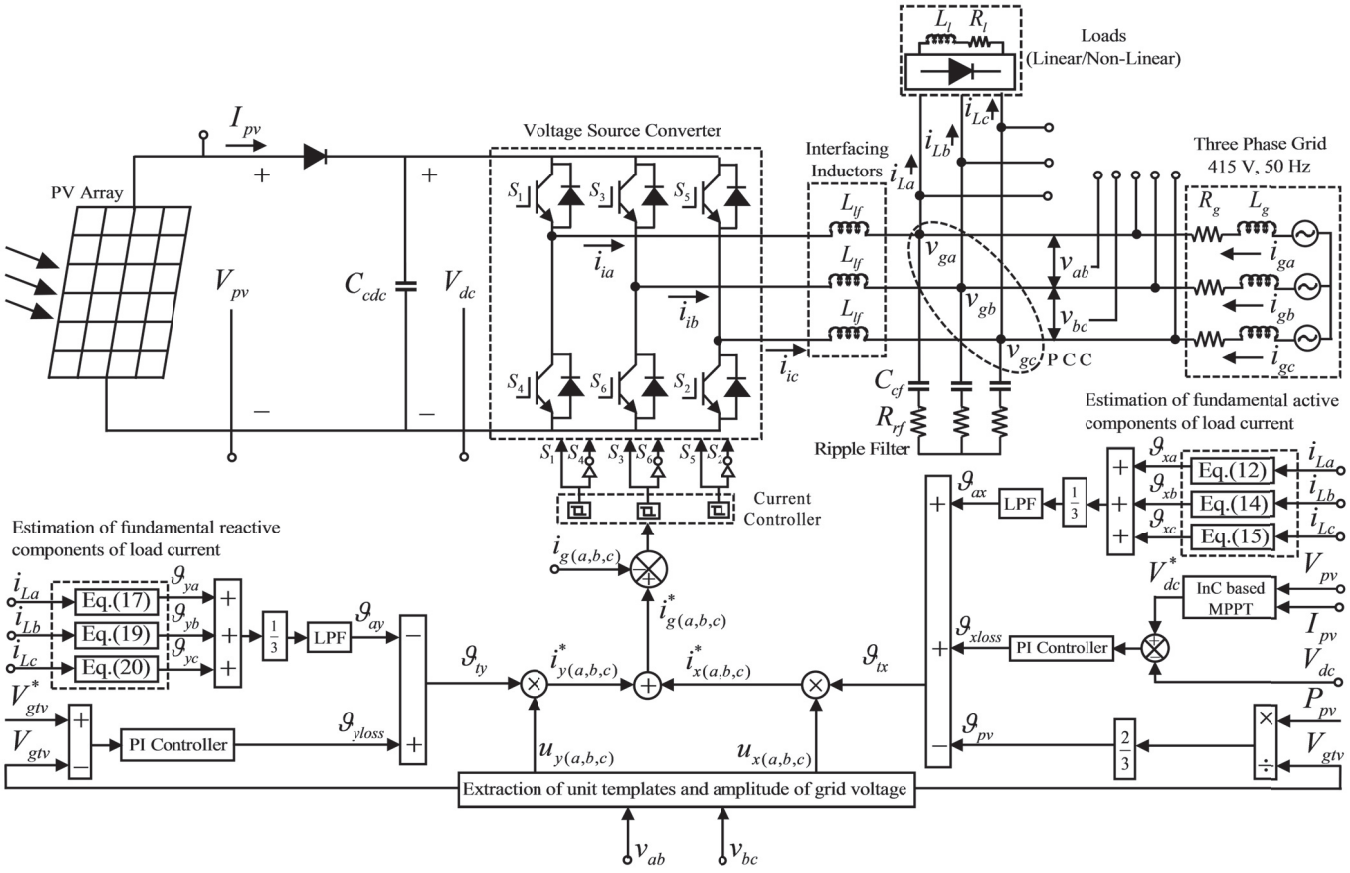

Fig. 1. Schematic of the grid-tied PV system with SLMF control

rate estimation of fundamental components (active and reactive) of nonlinear load currents even during dynamic conditions.

- Extraction of maximum power from PV modules and injecting the surplus power at Unity Power Factor (UPF) to the grid even during irradiation change.
- Compensation of harmonics injected by the loads connected at the PCC while maintaining the grid currents sinusoidal and balanced.
- Effective utilization of the VSC during night.

The paper is organized as follows. In Section II, the proposed SLMF based controller is discussed. In Section III, the schematic layout of the PV system along with the sensed signals and design of controller required for generation of reference grid current is discussed. To verify the efficacy of the proposed SLMF based control algorithm, simulation study is presented in Section IV. Finally, the paper is concluded in Section V.

II. Proposed SLMF based Controller

The cost function of the SLMF based control strategy is given as [9]:

$$J(l) = \frac{1}{\alpha(l)} S(l) = \frac{1}{\alpha(l)} \frac{1}{1 + e^{-\alpha(l) J_e(l)}} \tag{1}$$

where, $\alpha(l) = \alpha_k e^{-\bar{e}(l)}$ is the variable steepness parameter and $J_e(l) = E\left[e(l)^4\right]$ is the cost function of conventional LMF algorithm.

$$\bar{e}(l) = \gamma \bar{e}(l-1) + (1-\gamma) \Gamma k_e min(\mathbf{O}(l)) \tag{2}$$

where, k_e is a positive parameter, $0 \ll \gamma < 1$ is the leakage factor, the finite-sample correction factor $\Gamma = 1.483\,(1 + 5/(N_w - 1))$, N_w is the filter length, $\mathbf{O}(l) = [|e\,(l)|, \ldots, |e\,(l - N_w + 1)|]^T$ and $min(\cdot)$ is the minimum operator. The weight vector is then updated as [9]:

$$\vartheta(l+1) = \vartheta(l) + \rho \mathbf{\Lambda}(l) e(l)^3 u(l) \tag{3}$$

where, $\mathbf{\Lambda}(l) = S(l)\,(1 - S(l))$, can be thought of as a variable step size which provides fast convergence or lower steady-state misalignment and ρ is the step-size.

III. Design of Controller

Fig. 1 shows control strategy for a single-stage grid-tied PV system with SLMF based control. The following signals are sensed: PV voltage and current (V_{pv}, I_{pv}), PCC line voltage (v_{ab}, v_{bc}), three-phase inverter currents (i_{ia}, i_{ib}, i_{ic}), three-phase grid currents (i_{ga}, i_{gb}, i_{gc}) and three-phase load currents (i_{La}, i_{Lb}, i_{Lc}). Using the weight update equation (3), the proposed SLMF based control strategy is developed which comprises of five distinct steps.

A. Unit Template Generation

By sensing the line voltages (v_{ab}, v_{bc}) at the PCC, the phase voltages $(v_{g(a,b,c)})$ are evaluated as in [6]. The peak of the amplitude of the grid terminal voltage is then calculated as:

$$V_{gtv} = \sqrt{\frac{2}{3}(v_{ga}^2 + v_{gb}^2 + v_{gc}^2)} \tag{4}$$

The unit templates (in-phase and quadrature) are then given as [6]:

$$u_{xa} = \frac{v_{ga}}{V_{gtv}}; \quad u_{xb} = \frac{v_{gb}}{V_{gtv}}; \quad u_{xc} = \frac{v_{gc}}{V_{gtv}} \tag{5}$$

$$\begin{bmatrix} u_{ya} \\ u_{yb} \\ u_{yc} \end{bmatrix} = \frac{1}{\sqrt{3}} \begin{bmatrix} 0 & -1 & 1 \\ 3/2 & 1/2 & -1/2 \\ -3/2 & 1/2 & -1/2 \end{bmatrix} \begin{bmatrix} u_{xa} \\ u_{xb} \\ u_{xc} \end{bmatrix} \tag{6}$$

Improved dynamic performance in PV is achieved by adding a feed-forward term to the control strategy given as [6]:

$$\vartheta_{pv}(l) = \frac{2P_{pv}(l)}{3V_{gtv}} \tag{7}$$

where, P_{pv} is the power extracted from the PV.

B. Maximum Power Extraction

Maximum power from the PV is extracted using an InC MPPT control scheme. The operating point is updated referring to [10]. A proportional-integral (PI) controller regulates V_{dc} such that it follows V_{dc}^*.

C. Loss Component Estimation

The error of the DC-link voltage is given as:

$$V_{dc}^e(l) = V_{dc}^*(l) - V_{dc}(l) \tag{8}$$

The error of the DC-link voltage is fed to a PI controller which generates the DC loss component (ϑ_{xloss}):

$$\begin{aligned}\vartheta_{xloss}(l+1) = \vartheta_{xloss}(l) &+ P_{dc}[V_{dc}^e(l+1) - V_{dc}^e(l)] \\ &+ I_{dc}V_{dc}^e(l+1)\end{aligned} \tag{9}$$

where, I_{dc} and P_{dc} denotes the integral and proportional gains of DC-link PI controller.

Another PI controller controls the error of the grid terminal voltage at PCC (V_{gtv}^e) given as:

$$V_{gtv}^e(l) = V_{gtv}^*(l) - V_{gtv}(l) \tag{10}$$

where, $V_{gtv}^* = 340$ V is the reference terminal voltage. The output of the PI controller is the AC loss component (ϑ_{yloss}):

$$\begin{aligned}\vartheta_{yloss}(l+1) = \vartheta_{yloss}(l) &+ P_{ac}[V_{gtv}^e(l+1) - V_{gtv}^e(l)] \\ &+ I_{ac}V_{gtv}^e(l+1)\end{aligned} \tag{11}$$

where, I_{ac} and P_{ac} denotes the integral and proportional gains of grid terminal voltage PI controller.

D. Fundamental Component Extraction

The weight of the fundamental active component of the load current of phase 'a' is given as:

$$\vartheta_{xa}(l+1) = \vartheta_{xa}(l) + \rho_x \mathbf{\Lambda}_{xa}(l) e_{xa}^3(l) u_{xa}(l) \tag{12}$$

where, $\mathbf{\Lambda}_{xa}(l) = S_{xa}(l)\,(1 - S_{xa}(l))$, $\vartheta_{xa}(l)$ is the weight of the fundamental active component of load current of phase 'a' at the l^{th} instant, ρ_x is the active step-size and $e_{xa}(l)$ denotes the error of the adaptive active component at the l^{th} instant.

$$e_{xa}(l) = i_{La}(l) - u_{xa}(l) \times \vartheta_{xa}(l) \tag{13}$$

where, $i_{La}(l)$ is the load current of phase 'a' at the l^{th} instant. Similarly, the weight of fundamental active components of load currents of phase 'b' and 'c' are calculated as:

$$\vartheta_{xb}(l+1) = \vartheta_{xb}(l) + \rho_x \mathbf{\Lambda}_{xb}(l) e_{xb}^3(l) u_{xb}(l) \tag{14}$$

$$\vartheta_{xc}(l+1) = \vartheta_{xc}(l) + \rho_x \mathbf{\Lambda}_{xc}(l) e_{xc}^3(l) u_{xc}(l) \tag{15}$$

The average weight of the fundamental active component of load current is then evaluated as:

$$\vartheta_{ax} = \frac{(\vartheta_{xa} + \vartheta_{xb} + \vartheta_{xc})}{3} \tag{16}$$

The weight of the fundamental reactive component of the load current of phase 'a' is given as:

$$\vartheta_{ya}(l+1) = \vartheta_{ya}(l) + \rho_y \mathbf{\Lambda}_{ya}(l) e_{ya}^3(l) u_{ya}(l) \tag{17}$$

where, $\mathbf{\Lambda}_{ya}(l) = S_{ya}(l)\,(1 - S_{ya}(l))$, $\vartheta_{ya}(l)$ is the weight of the fundamental reactive component of load current of phase 'a' at the l^{th} instant, ρ_y is the reactive step-size and $e_{ya}(l)$ denotes the error of the adaptive reactive component at the l^{th} instant.

$$e_{ya}(l) = i_{La}(l) - u_{ya}(l) \times \vartheta_{ya}(l) \tag{18}$$

where, $i_{La}(l)$ is the load current of phase 'a' at the l^{th} instant. Similarly, the weight of fundamental reactive components of load currents of phase 'b' and 'c' are calculated as:

$$\vartheta_{yb}(l+1) = \vartheta_{yb}(l) + \rho_y \mathbf{\Lambda}_{yb}(l) e_{yb}^3(l) u_{yb}(l) \tag{19}$$

$$\vartheta_{yc}(l+1) = \vartheta_{yc}(l) + \rho_y \mathbf{\Lambda}_{yc}(l) e_{yc}^3(l) u_{yc}(l) \tag{20}$$

The average weight of the fundamental reactive component of load current is then evaluated as:

$$\vartheta_{ay} = \frac{(\vartheta_{ya} + \vartheta_{yb} + \vartheta_{yc})}{3} \tag{21}$$

E. Reference Grid Current Estimation and Gate Pulse Generation

The net fundamental active power component (ϑ_{tx}) and reactive power component (ϑ_{ty}) of reference grid current is calculated as per a sign convention and are given as:

$$\vartheta_{tx} = \vartheta_{ax} + \vartheta_{xloss} - \vartheta_{pv} \tag{22}$$

$$\vartheta_{ty} = \vartheta_{yloss} - \vartheta_{ay} \tag{23}$$

TABLE I
SIMULATION PARAMETERS OF THE GRID-TIED PV SYSTEM

Symbol	Parameter	Value
V_{mpp}	Voltage of PV array at maximum power	749.275 V
I_{mpp}	Current of PV array at maximum power	13.62 A
P_{mpp}	PV array maximum power at 1000 W/m^2	10.2 kW
V_{dc}	DC-bus voltage	700 V
L_{if}	Interfacing filter inductance	9 mH
C_{dc}	DC-bus capacitance	2350 μF
V_{LL}	Grid line voltage	415 V
R_{rf}	Ripple Filter Resistance	5 Ω
C_{rf}	Ripple Filter Capacitance	5 μF
P_{dc}	Proportional gain of DC PI regulator	0.42
I_{dc}	Integral gain of DC PI regulator	1.2
P_{ac}	Proportional gain of AC PI regulator	0.42
I_{ac}	Integral gain of AC PI regulator	1.2
ρ_x	Active learning rate	0.0002
ρ_y	Reactive learning rate	0.0002
R_l, L_l	Resistance and Inductance of the R-L load	98.6 Ω, 211.8 mH
T_s	Sampling Time	6 μs

The active reference grid current $\left(i^*_{x(a,b,c)}\right)$ and reactive reference grid current $\left(i^*_{y(a,b,c)}\right)$ are then evaluated as:

$$i^*_{x(a,b,c)} = \vartheta_{tx} \cdot u_{x(a,b,c)} \tag{24}$$

$$i^*_{y(a,b,c)} = \vartheta_{ty} \cdot u_{y(a,b,c)} \tag{25}$$

The reference grid currents are then calculated as

$$i^*_{g(a,b,c)} = i^*_{x(a,b,c)} + i^*_{y(a,b,c)} \tag{26}$$

For switching of the VSI, a Hysteresis Controller (HC) is used. The width of the HC is considered as 0.01 and is fed with the error signal of current given as:

$$i^e_{g(a,b,c)} = i^*_{g(a,b,c)} - i_{g(a,b,c)} \tag{27}$$

IV. RESULTS AND DISCUSSION

A 10 kW grid-tied PV system is simulated using MATLAB/Simulink. The PV array comprises of 25 series PV modules and 4 strings in parallel. The parameters used for simulation are presented in Table I. A non-linear load of 3.2 kW is represented by a diode-bridge rectifier in series with a R-L load.

A. Performance During Variable Irradiation

The dynamic performance of the grid-tied PV system during variable irradiation is analyzed under two conditions:

1) Irradiation change to 800 *W/m² from* 1000 *W/m²:* The dynamic response of the PVS-UG during irradiation change is shown in Fig. 2(a)-(b). A step-change in solar irradiation (G_{pv}) is made to 800 W/m^2 from 1000 W/m^2 for the time duration $t = 0.5$ s to $t = 0.55$ s. As irradiation drops, the available power from the PV reduces from 10.2 kW to 8.16 kW. The active power injected to the grid (P_g) is thus reduced from 7 kW to 4.96 kW. The grid current injected per phase (i_{gabc}) is therefore reduced but it is at a phase difference of 180° with the grid phase voltage (v_{gabc}). The inverter current (i_{iabc}) and PV current (I_{pv}) are also reduced instantly. The DC-link voltage (V_{dc}) changes and settles at its set value. The intermediate signals ϑ_{ax}, ϑ_{xloss}, ϑ_{pv} and ϑ_{tx} are given in Fig. 2(b). No change is seen in ϑ_{ax}, since it is the load parameter and independent of changes in irradiation. ϑ_{pv} drops since it depends on the irradiation (G_{pv}). ϑ_{tx} calculates the active power to be exchanged by the grid. Hence, during irradiation change to 800 W/m^2 from 1000 W/m^2, ϑ_{tx} also reduces and the negative sign indicates power being injected to the grid.

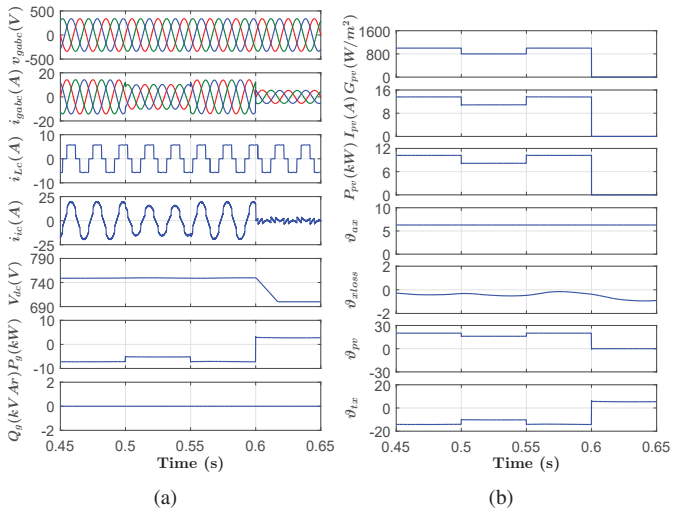

Fig. 2. Dynamic Response during variable irradiation (a) waveforms of grid-tied PV system (b) PV and intermediate signals

2) Zero Irradiation: The dynamic performance of the PVS-UG during zero irradiation (when PV power is unavailable) is given in Fig. 2(a)-(b). At $t = 0.6$ s solar irradiation (G_{pv}) drops to 0 W/m^2 from 1000 W/m^2. After step-change in irradiation, the available power from PV becomes zero. The active power demand of the load is now met by the grid. Thus, active power delivered by the grid (P_g) is 3.2 kW. The grid current per phase (i_{gabc}) is therefore further reduced but is now in phase with the phase voltage of grid (v_{gabc}) since power is being supplied by the grid. The PV current (I_{pv}) drops to zero instantly and the DC-link voltage (V_{dc}) drops and settles at the desired value. When irradiation drops to 0 W/m^2, the VSC mitigates the injected load harmonics. This shows that the VSC is used effectively even during night when PV power is unavailable. The intermediate signals ϑ_{ax}, ϑ_{xloss}, ϑ_{pv} and ϑ_{tx} are given in Fig. 2(b). No change is seen in ϑ_{ax}, since it is the load average weight component and independent of irradiation change. ϑ_{pv} depends on I_{pv}, thus it falls to zero. ϑ_{tx} calculates the active power to be exchanged by the grid. Hence, during irradiation change to 0 W/m^2 from 1000 W/m^2, ϑ_{tx} changes to positive from negative value indicating power being supplied by the grid. The tracking performance of the DC Bus voltage during zero irradiation is given in Fig. 3(a).

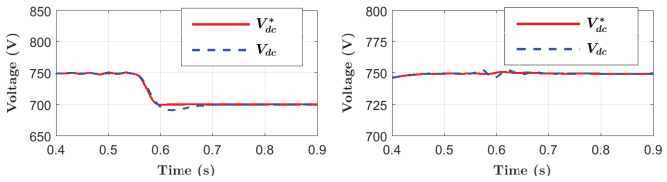

Fig. 3. DC-Bus voltage vs. reference DC-Bus voltage(a) During variable irradiation (b) During unbalanced nonlinear load

B. Performance During Load Unbalancing

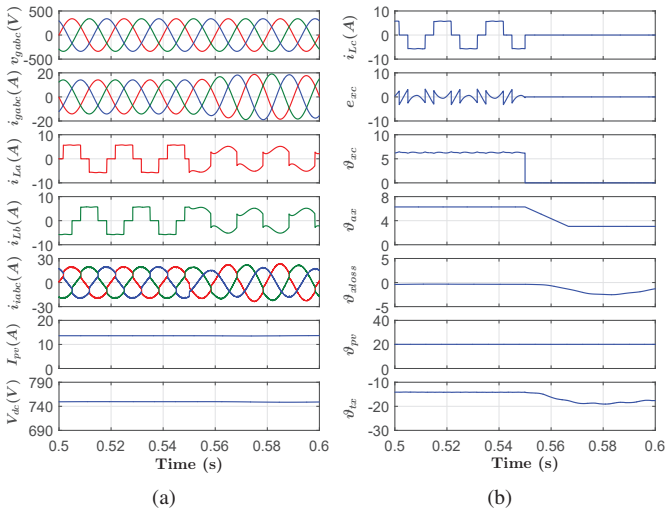

Fig. 4. Dynamic Response during load unbalancing (a) waveforms of grid-tied PV system (b) Phase 'c' load current and intermediate signals

The dynamic performance of the PVS-UG with unbalanced nonlinear load is shown in Fig. 4. At $t = 0.55$ s, 'c' phase load is cut-off which is represented in the response of i_{Lc}. During unbalancing of load, the load demand reduces, thus an increment is seen in grid current (i_{gabc}) waveform as more power gets injected to the grid. The grid currents are maintained sinusoidal, balanced and at UPF even though the load currents are unbalanced. The DC-link voltage (V_{dc}) is maintained constant at the desired value. The phase 'a' and 'b' inverter current increases whereas the inverter current of phase 'c' reduces. During unbalancing of load, the adaptive component of error of phase 'c' (e_{xc}) becomes zero and the weights $(\vartheta_{xc}, \vartheta_{ax}, \vartheta_{xloss}$ and $\vartheta_{tx})$ changes and then stabilize to their desired value as given in Fig. 4(b). No change is seen in the PV feed-forward component ϑ_{pv}, since it is independent of load variations. The tracking performance of the DC Bus voltage during unbalanced load is given in Fig. 3(b).

C. Comparative Analysis of the Proposed SLMF Control with Conventional Control

The response of average fundamental active weight component (ϑ_{ax}) of the proposed SLMF control scheme and conventional LMF control scheme when subjected to load unbalancing in phase 'c' is presented in Fig. 5. The proposed SLMF based control shows less oscillations in 'ϑ_{ax}' compared to conventional LMF based control. The waveforms show better accuracy and fast convergence of the proposed SLMF based control. A comparative study of the proposed SLMF control with conventional LMF based control is provided in Table II. The THD of compensated grid current using LMF and SLMF control is given in Fig. 6-7. Fig. 8 shows the THD of the load current.

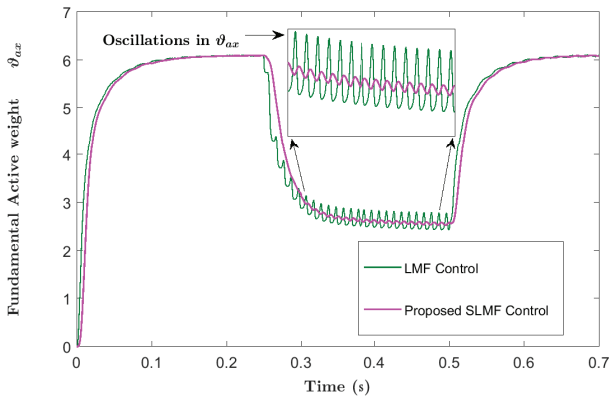

Fig. 5. Response of ϑ_{ax} for proposed SLMF and conventional LMF based control

TABLE II
COMPARATIVE ASSESSMENT OF THE PROPOSED SLLAD CONTROL WITH EXISTING CONTROL

Control Algorithm	Complexity (multiplication)	Oscillation (in weights)	THD % (grid current)
LMF	$3N$+7	High	3.7
Proposed SLMF	$2N$+7	Low	2.9

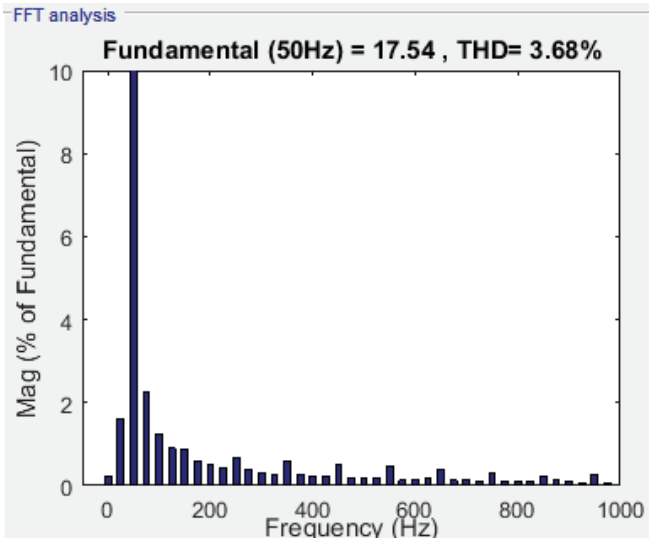

Fig. 6. Grid current THD using LMF control

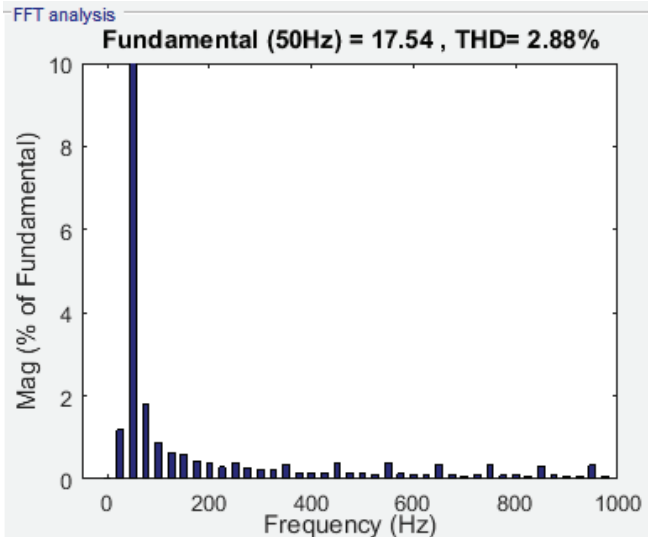

Fig. 7. Grid current THD using SLMF control

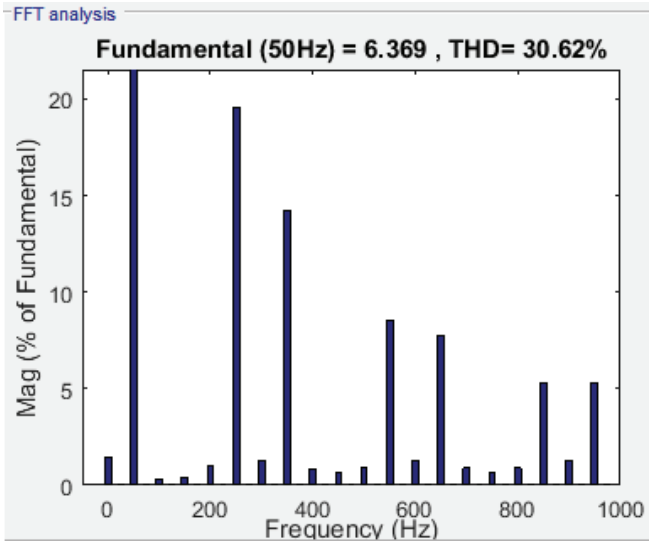

Fig. 8. THD of load current

V. Conclusion

In this paper, a new SLMF based control scheme for a grid-tied PV system is proposed. The proposed control scheme mitigates the injected load harmonics thereby improving the power quality during during dynamic conditions such as load unbalancing and variable irradiation. The performance of the proposed control scheme is validated in simulation using MATLAB/Simulink. The response of the grid-tied PV system was found to be better than its conventional counterpart in terms of improved robustness during dynamic conditions, faster convergence, less steady-state misalignment and lesser oscillation in weights. The grid-tied PV system operates at UPF maintaining the grid currents balanced even during irradiation change and load unbalancing conditions. During night (when PV power is unavailable), the VSI compensates the harmonics of load. Thus, VSI is used effectively even during unavailability of PV power. The improvement in PQ is seen in terms of lower THD which is well within the IEEE-519 standards.

Acknowledgment

The authors would like to thank DST, Govt. of India for supporting the research vide no. DST/INT/Thai/P-12/2019.

References

[1] J. Dulac, M. LaFrance, N. Trudeau, and H. Yamada, "Transition to sustainable buildings: Strategies and oppourtunities to 2050," *International Energy Agency OECD/IEA, Ed., Paris, France.*, 2013.

[2] A. K. Barnes, J. C. Balda, and C. M. Stewart, "Selection of converter topologies for distributed energy resources," in *2012 27th Annual IEEE Applied Power Electronics Conference and Exposition (APEC)*. IEEE, 2012, pp. 1418–1423.

[3] X. Liang, "Emerging power quality challenges due to integration of renewable energy sources," *IEEE Transactions on Industry Applications*, vol. 53, no. 2, pp. 855–866, 2016.

[4] M. Quraan, "Error compensation algorithm for srf-pll in three-phase grid-connected converters," *IEEE Access*, vol. 8, pp. 182 338–182 346, 2020.

[5] Z. Ali, N. Christofides, K. Saleem, A. Polycarpou, and K. Mehran, "Performance evaluation and benchmarking of pll algorithms for grid-connected res applications," *IET Renewable Power Generation*, vol. 14, no. 1, pp. 52–62, 2019.

[6] R. K. Agarwal, I. Hussain, and B. Singh, "Lmf-based control algorithm for single stage three-phase grid integrated solar pv system," *IEEE Transactions on Sustainable Energy*, vol. 7, no. 4, pp. 1379–1387, 2016.

[7] A. Bag, B. Subudhi, and P. K. Ray, "An adaptive variable leaky least mean square control scheme for grid integration of a pv system," *IEEE Transactions on Sustainable Energy*, vol. 11, no. 3, pp. 1508–1515, 2020.

[8] P. Shukl and B. Singh, "Combined iir and fir filter for improved power quality of pv interfaced utility grid," *IEEE Transactions on Industry Applications*, 2020.

[9] F. Huang, J. Zhang, and S. Zhang, "A family of robust adaptive filtering algorithms based on sigmoid cost," *Signal Processing*, vol. 149, pp. 179 – 192, 2018.

[10] B. Subudhi and R. Pradhan, "A comparative study on maximum power point tracking techniques for photovoltaic power systems," *IEEE Transactions on Sustainable Energy*, vol. 4, no. 1, pp. 89–98, 2012.